
Comparison of Rigid and Flexible Simple Point Charge Water Models at Supercritical Conditions

TAHMID I. MIZAN, PHILLIP E. SAVAGE,* and ROBERT M. ZIFF

Department of Chemical Engineering, University of Michigan, Ann Arbor, Michigan 48109-2136

Received 31 October 1995; accepted 1 February 1996

ABSTRACT

This study investigates the differences between the predictions of various properties of rigid and flexible simple point charge water models at supercritical conditions. Molecular dynamics simulations were conducted for supercritical water in a temperature range of 773–1073 K and densities in the range 115–659 kg/m³. We present thermodynamic data, pair correlation functions, self-diffusivity, power spectra, dielectric constants, and various measures of hydrogen bonding at different state conditions. The flexible water model performs better in predicting the pressures along the supercritical isotherms simulated. Agreement between experimental and calculated dielectric constants is superior for the flexible water model, particularly at high densities. The flexible model exhibits a greater degree of hydrogen bonding and more persistent hydrogen bonds than does the rigid model. The structural features of supercritical water at high densities are identical for the two water models. At low densities, however, the flexible potential exhibits pair correlation functions with enhanced peaks. Inclusion of flexibility in the potential model does not result in a significant shift in the position of the rotational/librational peak in the power spectrum. The self-diffusivities obtained from the simulations are within the accuracy of the experimental values for both the rigid and flexible models. On balance the inclusion of flexibility improves agreement with the properties of real supercritical water while incurring little or no additional computational burden. © 1996 by John Wiley & Sons, Inc.

*Author to whom all correspondence should be addressed.
E-mail: psavage@engin.umich.edu

Introduction

Since the seminal work of Rahman and Stillinger¹ a large number of rigid and flexible water models have been used to simulate the properties of water using molecular dynamics or Monte Carlo techniques. Traditionally these simulations were of liquid water, but more recently several studies of supercritical water (SCW) have been published.²⁻⁵ Scientific interest in SCW is a relatively new development and has arisen primarily out of its role as a versatile and environmentally benign reaction medium.⁶

Most molecular dynamics studies of both pure SCW^{3,7} and, aqueous supercritical solutions^{4,8-15} have used rigid water models such as the simple point charge (SPC)¹⁶ or TIP4P.¹⁷ A number of liquid water¹⁸⁻²⁵ and SCW^{5,26,27} simulations with flexible models have also been reported, however. These provide evidence that suggests that flexibility, or inclusion of intramolecular degrees of freedom, in a water model tends to produce more realistic behavior than does a rigid water model. Other potential benefits of including flexibility are discussed elsewhere.⁵ Moreover, efficient computational methods to treat these additional degrees of freedom effectively are now available.²⁸ In the present study we compare various properties of the rigid SPC water model to its flexible counterpart to facilitate meaningful comparison and interpretation of the results of rigid SCW simulations and flexible SCW simulations reported in the literature. Moreover, we investigate the effect of flexibility on various properties and demonstrate that the inclusion of flexibility is advantageous for simulation of certain properties.

SPC Potential Models for Water

The rigid water model we used is the SPC model potential.¹⁶ In this study, the expanded form will be used to describe the generic case, while the acronym will be reserved exclusively for the specific model proposed by Berendsen et al.¹⁶ The SPC water model has three point charges located at the three atoms. The model molecule interacts electrostatically with charges on other molecules through these charges located on its atomic sites. It also has a Lennard-Jones interac-

tion potential centered at the oxygen atom whereby it can interact with similar potential sites on other molecules. The SPC model has a rigid geometry (fixed bond lengths and bond angle), and molecular dynamics simulations must treat it as rigid rotor. The HOH bond angle of the monomer is 109.5° rather than the 104.5° equilibrium angle of real water.²⁹ Moreover, the OH bond length is 1 Å in the SPC model as opposed to 0.957 Å, which is the equilibrium OH bond length in real water.²⁹

To investigate the effect of intramolecular degrees of freedom on the properties of SCW we used a flexible version of the SPC model originally used by Teleman et al.²⁵ to simulate liquid water. We refer to this model as the TJE (Teleman-Jönsson-Engström) model. The intermolecular part of the TJE potential is identical to the SPC model. In addition, it has an intramolecular part consisting of simple harmonic terms corresponding to the bending and stretching modes of the water molecule. The numerical values of the potential parameters are given elsewhere.²⁵ The geometry of the TJE water molecule depends on the density and temperature, so it can differ from its reference geometry (that of the SPC model). Thus, the relative placement of its charges, and hence its dipole moment, can also change with the state conditions. On average, it has a dipole moment higher than that of the SPC model except in very rarefied systems.

The main focus of this study is the comparison of the properties of the TJE model with the SPC model under supercritical conditions. Except where otherwise stated, the terms flexible model and rigid model refer to the TJE and SPC models, respectively.

Simulation Techniques

All simulations were carried out using 256 molecules in a cubic cell of constant volume using standard molecular dynamics techniques.³⁰ Periodic boundary conditions were used for all runs except those used to calculate self-diffusivity. The cutoff was based on molecular center of mass distance. A molecular cutoff ensures neutrality of charge. An automatically updated molecular neighbor list was employed. Except where otherwise mentioned, long-range Coulomb interactions were treated using the reaction field method, in which the external dielectric constant defining

the reaction field, ϵ_{RF} , was arbitrarily chosen to be 80. No long-range correction was made for the Lennard-Jones term of the intermolecular potential.

Supercritical water was simulated using both the rigid and flexible models along the 773 and 1073 K isotherms at densities of 115, 257, 406, and 659 kg/m³ and along 257 and 659 kg/m³ isochores at temperatures of 773, 873, 973, and 1073 K. The systems were equilibrated for at least 100 ps. The memory and storage limitations of our computing environment necessitated separate runs for properties requiring different sampling times or different total run lengths. Production runs were of 100 ps duration for structural and energetic data, 200 ps for dielectric data, 20 ps for self-diffusivity data, and 2.1 ps for velocity autocorrelation data. The simulation box sizes were 40.5 Å (18-Å cutoff) and 31 Å (14-Å cutoff) for the two low SCW densities and 26.6 Å (12-Å cutoff) and 22.6 Å (10-Å cutoff) for the two high-density states, respectively.

For the flexible TJE model, the equations of motion were integrated using the reversible reference system propagator algorithm (r-RESPA).²⁸ This multiple time step method treats rapidly varying forces, such as those responsible for bond stretch, in the short time step, while considering the slowly varying forces at the long time step intervals. The algorithm was implemented in Cartesian coordinates. We considered bond stretching forces at each short time step interval and all other forces, namely, bond-angle bending forces and nonbonded forces, at every long time step interval. The long time step was set at 2 fs and the short time step at 0.25 fs. Separate temperature scaling was applied to translational, rotational, and internal degrees of freedom^{5,18} at every long time step following the method of Berendsen et al.³¹ and using a relaxation time constant of 6 fs to maintain the temperature at around the desired value.

The method used for the rigid water simulations was identical to that used for the flexible water simulations except for the features discussed below. We used the rigid SPC¹⁶ model for all rigid water simulations. The equations of motion were integrated using the RATTLE method.³² This is essentially an implementation of the velocity Verlet method incorporating a constraint algorithm. A time step of 2 fs was used (except where otherwise stated). Again, separate temperature scaling was applied to translational and rotational degrees of freedom at every time step.

It is noteworthy that the r-RESPA method was about 7% faster than RATTLE at the same state condition (115 kg/m³, 773 K), with the same cut-off, and on the same computer (HP 715/64). Thus, r-RESPA is at least as efficient as RATTLE, even though it takes into account many more degrees of freedom.

The power spectra for the TJE and SPC models were calculated at one state point from NVE simulation trajectories. The Ewald summation method, which has better energy conservation characteristics than the reaction field method, was used to treat long-range Coulombic interactions for these simulations. The expression for the Ewald summation contribution to the potential energy is^{30,33,34}

$$\begin{aligned}
 U^{\text{Ewald}} = & \frac{1}{4\pi\epsilon_0} \sum_{\mathbf{n}} \sum_m^{N_m} \sum_{l>m}^{N_m} \sum_i^{N_a} \sum_{j \neq i}^{N_a} q_i q_j \\
 & \times \frac{\text{erfc}(\alpha|\mathbf{r}_{ij} + \mathbf{n}|)}{|\mathbf{r}_{ij} + \mathbf{n}|} \\
 & + \frac{1}{2\epsilon_0 V} \sum_{\mathbf{k} \neq 0} \frac{1}{k^2} e^{-k^2/4\alpha^2} \left\| \sum_m^{N_m} \sum_i^{N_a} q_i e^{\mathbf{k} \cdot \mathbf{r}_i} \right\|^2 \\
 & - \frac{\alpha}{4\pi^{3/2}\epsilon_0} \sum_m^{N_m} \sum_i^{N_a} q_i^2 \\
 & - \frac{1}{4\pi\epsilon_0} \sum_m^{N_m} \sum_{\kappa}^{N_a} \sum_{\lambda > \kappa}^{N_a} q_{n\kappa} q_{n\lambda} \frac{\text{erf}(\alpha|\mathbf{r}_{\kappa\lambda}|)}{|\mathbf{r}_{\kappa\lambda}|}, \quad (1)
 \end{aligned}$$

where i , κ , or λ is the index of an atom on molecule m , and j is the index of an atom on molecule l . Here α is chosen large enough so that only the $|\mathbf{n}| = 0$ term contributes to the real space sum. The last term in eq. (1) is a correction term for the intramolecular self-energy. This term is constant for rigid molecules. For molecules having intramolecular flexibility, however, the intramolecular site-site distances $\mathbf{r}_{\kappa\lambda}$ will change from one instant to another and hence this term must be evaluated and subtracted at each time step. A shifted-force Lennard-Jones interaction term was used to achieve even better energy conservation. Also, the long time step was set to 1 fs and the short time step to 0.25 fs for the flexible water simulation using r-RESPA to obtain improved energy conservation and also to obtain better resolution of the high frequency motions. A time step of 0.5 fs was used for the NVE simulation of rigid water using RATTLE.

Results and Discussion

The thermodynamic properties, hydrogen bonding measures, structure, dielectric properties, self-diffusivities, and power spectra of simulated water were calculated at supercritical conditions. The results are discussed below.

THERMODYNAMIC PROPERTIES

Table I compares the thermodynamic properties obtained for SCW using the TJE and SPC potential models at 773 K. The uncertainties in Table I are the standard deviations. The pressures we calculated were close to the experimental values³⁵ for the two low density states and higher than the experimental values at the two higher densities. This trend is also depicted graphically in Figure 1. The two low density state points almost coincide with the 773 and 1073 K isotherms for both the TJE and SPC models. At high densities both models diverge from the experimental isotherms, but the discrepancy for the SPC model is greater. Similar results were also obtained at temperatures intermediate to the isotherms shown in Figure 1. The proximity of the simulated TJE data points and experimental isotherm suggests that the isotherm of TJE water might be close to that of real water. This, in turn, suggests that the critical point of TJE water may lie closer to the critical point of real water than does the critical point of SPC water. The results indicate that the TJE model is superior to the SPC model in simulating the gross PVT properties of SCW under reaction field conditions.

The configurational potential energy, U_{pot} for the flexible potential was about 7 kJ/mol more positive than the experimental value³⁵ at each state point, whereas the rigid SPC potential produced fairly good agreement. The differences in potential energy between states, however, are in close agreement with the experiment for both models. Comparison of experimental potential energies with the corresponding intermolecular potential energy reveals that better agreement is obtained if the intramolecular part of the potential energy is not considered for the flexible model.

DIMER ENERGIES

Dimer energies or pair energies are the energies of interaction experienced by any two molecules in the system. An investigation of pair energies may

TABLE I.
Thermodynamic Properties of Supercritical Water at 773 K.

Property	State 1a		State 2a		State 3a		State 4a	
	TJE	SPC	TJE	SPC	TJE	SPC	TJE	SPC
ρ (kg/m ³)	115.26		257.0		405.8		659.3	
P (exptl ³⁵) (bar)	300		500		700		1717	
P (simulation) (bar)	274 ± 58	295 ± 51	485 ± 167	560 ± 159	775 ± 313	927 ± 287	2121 ± 610	2495 ± 568
Exptl U_{pot}^{35} (kJ/mol)	-5.6		-10.9		-15.1		-21.1	
$\langle U_{\text{pot}} \rangle$ (kJ/mol)	1.9 ± 0.6	-7.0 ± 0.5	-3.8 ± 0.6	-12.3 ± 0.6	-8.0 ± 0.6	-16.2 ± 0.6	-13.6 ± 0.6	-21.6 ± 0.5
$\langle U_{\text{inter}} \rangle$ (kJ/mol)	-8.4 ± 0.6	-7.0 ± 0.5	-14.4 ± 0.7	-12.3 ± 0.6	-18.8 ± 0.7	-16.2 ± 0.6	-24.9 ± 0.6	-21.6 ± 0.5
$\langle U_{\text{intra}} \rangle$ (kJ/mol)	10.3 ± 0.2		10.6 ± 0.2		10.9 ± 0.3		11.3 ± 0.3	

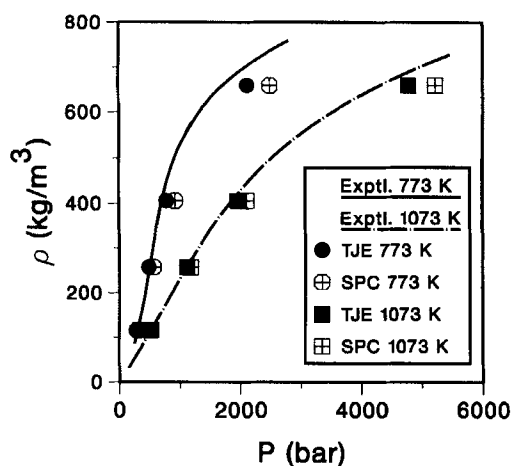


FIGURE 1. Isotherms for supercritical water at 773 and 1073 K.

shed light on the energetic environment experienced by a typical water molecule. Figure 2 shows the distribution of pair energies for the TJE and SPC water models at a typical supercritical state (257 kg/m^3 , 773 K). Also shown are the pair energy distribution curves for the two models at ambient liquid conditions. In contrast to the liquid water pair energy distributions, which are bimodal, the distributions for SCW are unimodal. At supercritical conditions both models exhibit a broad, sloping shoulder on the negative branch of the distribution. However, the negative branch of the pair energy distribution of the flexible potential has a gentler slope that extends to more negative pair energies. As discussed below, this is indicative of greater hydrogen bonding (based on an energetic criterion) in the flexible model. The pair

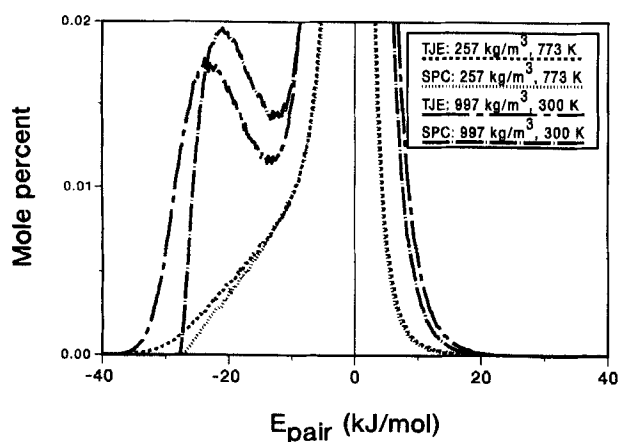


FIGURE 2. Pair energy distributions for TJE and SPC water models at ambient and supercritical conditions.

energy distribution curves shown in Figure 2 are typical of supercritical conditions and similar to curves obtained at other supercritical state conditions.

Another indicator of the energetic environment around a molecule is the trajectory-averaged dimer energy as a function of molecular separation, $E_{\text{pair}}(r)$. These are plotted for the rigid and flexible models at the representative supercritical state of 257 kg/m^3 and 773 K in Figure 3. The $E_{\text{pair}}(r)$ curves for the two models at liquid water conditions are also plotted in Figure 3 for reference. The well depths of the $E_{\text{pair}}(r)$ curves for the TJE model are greater than those of the SPC model. The dimer energy function, $E_{\text{pair}}(r)$, comprises both Lennard-Jones and Coulombic contributions. While the Lennard-Jones part is identical for both models, the Coulombic part is not. The root of the different well depths then lies in the flexible model, allowing the HOH angle and hence the dipole moment of the water molecule to change with density,⁵ while the rigid model molecule has a fixed dipole moment. The larger dipole moment of the flexible monomer translates into greater short-ranged attractive interactions between molecular pairs as reflected by the deeper $E_{\text{pair}}(r)$ potential wells.

HYDROGEN BONDING

We use an energetic criterion¹ to identify hydrogen bonds in SCW. In this method a hydrogen bond is said to exist if the pair interaction energy, E_{pair} , between two molecules is less than a negative threshold value, $E_{\text{HB,cut}}$, usually taken to be

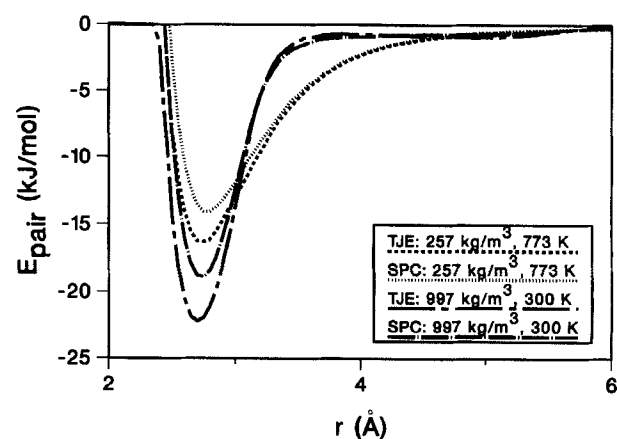


FIGURE 3. Pair energies as a function of molecular separation for TJE and SPC water models at ambient and supercritical conditions.

the minimum between the two peaks of the bimodal pair energy distribution of ambient water as shown in Figure 2. For the flexible potential model used in our study, $E_{\text{HB,cut}}$ is -13.2 kJ/mol, whereas for the rigid version of this model $E_{\text{HB,cut}}$ is -12.5 kJ/mol. Below we discuss various measures of hydrogen bonding in SCW for the two water models. Details of the calculation methods for these measure of hydrogen bonding may be found elsewhere.^{27,36}

Degree of Hydrogen Bonding

The degree of hydrogen bonding in water is often represented by, n_{HB} , which is the number of hydrogen bonds per water molecule averaged over all configurations sampled. Tables II and III give n_{HB} and various energetic measures of hydrogen bonding at different state points. These data show that n_{HB} is smaller and the hydrogen bonding energy less negative for SPC water than for TJE water at the same conditions. Both trends may be explained by considering the pair energy distributions for the two water models. For the flexible model the attractive branch of the pair energy distribution extends to more negative values and generally has a gentler slope. The area under this curve for pair energies more negative than $E_{\text{HB,cut}}$ is proportional to the number of hydrogen bonded molecular pairs. Even though $E_{\text{HB,cut}}$ is more negative for the TJE model, the area under the pair energy distribution curve is greater resulting in n_{HB} being greater. Similarly, these molecular pairs sample more negative energies resulting in the more negative average hydrogen bonding energies. It should be noted that most of the difference in hydrogen bonding energies is a result of the

difference in Coulombic interactions between molecular pairs. However, the Lennard-Jones portion of the hydrogen bonding energy is also smaller for the rigid SPC model than for the flexible TJE model. Since both models have identical Lennard-Jones terms, this difference must be ascribed to a difference in the average molecular spacing of the hydrogen bonded pairs. Thus, on average, hydrogen bonded pairs are closer together for the flexible model, because of the more attractive Coulombic interactions that result from the greater dipole moments of the monomers.

Cluster Size Distribution

Hydrogen bonded molecular pairs may form clusters of mutually bonded molecules. Characteristics of hydrogen bonded clusters for TJE water in SCW were examined previously.^{27,36} Here we look at the differences between hydrogen bonded clusters of rigid SPC water and flexible TJE water at supercritical conditions. Figure 4 plots the cumulative number fractions of clusters of size N , S_N , for two different densities at a temperature of 773 K. As is evident from the figure, differences between the cluster size distributions obtained using the two models are slight at best. The SPC model has a greater number of free or unbound molecules and a slightly narrower distribution at both the densities reported.

Hydrogen Bond Persistence Times

Hydrogen bonding is a dynamic phenomenon. At any instant in time some hydrogen bonds are being made while others are being broken. In all this frenetic activity an average or equilibrium

TABLE II.
Hydrogen Bond Analyses of Supercritical Water at 257 kg/m³.

Property	State 2a		State 2b		State 2c		State 2d	
	TJE	SPC	TJE	SPC	TJE	SPC	TJE	SPC
T (K)	773		873		973		1073	
n_{HB}	0.80	0.70	0.67	0.58	0.57	0.50	0.50	0.44
$\langle E_{\text{HB,Coulomb}} \rangle$ (kJ/mol)	-23.48	-21.07	-23.08	-20.66	-22.76	-20.41	-22.59	-20.21
$\langle E_{\text{HB,LJ}} \rangle$ (kJ/mol)	4.22	3.70	4.07	3.55	3.92	3.46	3.87	3.40
$\langle E_{\text{HB}} \rangle$ (kJ/mol)	-19.27	-17.36	-19.02	-17.11	-18.85	-16.85	-18.72	-16.82
τ_{HB} (ps)	0.1005	0.0950	0.0860	0.0794	0.0757	0.0727	0.0677	0.0647

LJ, Lennard-Jones.

HB, Hydrogen bond

TABLE III.
Hydrogen Bond Analyses of Supercritical Water at 659 kg/m³.

Property	State 4a		State 4b		State 4c		State 4d	
	TJE	SPC	TJE	SPC	TJE	SPC	TJE	SPC
<i>T</i> (K)	773		873		973		1073	
<i>n</i> _{HB}	1.44	1.29	1.32	1.17	1.22	1.08	1.14	1.00
$\langle E_{\text{HB,Coulomb}} \rangle$ (kJ/mol)	-24.12	-21.49	-23.78	-21.17	-23.51	-20.92	-23.33	-20.73
$\langle E_{\text{HB,LJ}} \rangle$ (kJ/mol)	4.65	4.08	4.52	3.96	4.41	3.88	4.34	3.80
$\langle E_{\text{HB}} \rangle$ (kJ/mol)	-19.47	-17.41	-19.26	-17.22	-19.10	-17.04	-18.99	-16.93
τ_{HB} (ps)	0.0860	0.0781	0.0727	0.0680	0.0639	0.0585	0.0564	0.0510

picture emerges. The measures of hydrogen bonding discussed above refer to a time-averaged description of the SCW system. In this section, however, we address the time intervals between making and breaking hydrogen bonds. One measure of the temporal characteristics of hydrogen bonding is how long a particular bond survives before a rupture occurs. This interval of time may be called the persistence time or lifetime of a hydrogen bond. If a hydrogen bond is present at time 0 and exists continuously (within the resolution of the data sampling period) until time *t*, it is said to persist at time *t*. A statistically significant value of this measure may be calculated using the following autocorrelation function originally devised by Rapaport³⁷

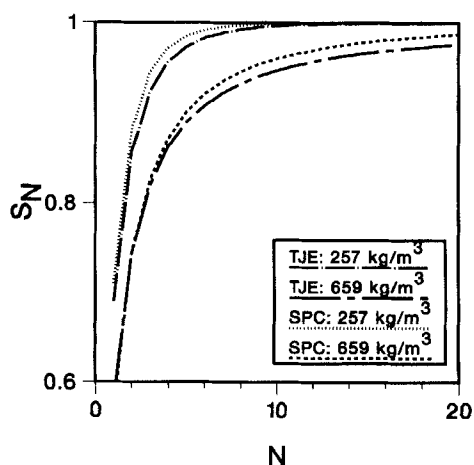
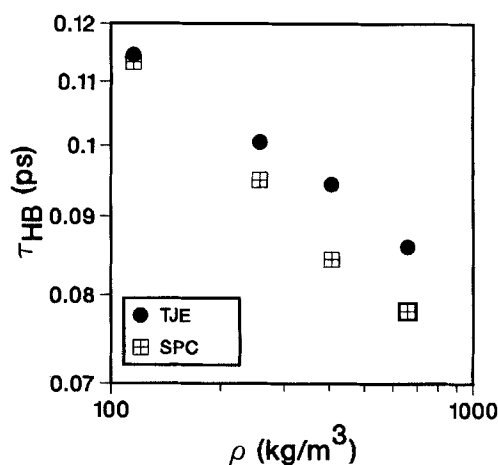
$$C_{\text{HB}}(t) = \frac{\sum_{\langle m,l \rangle} s_{m,l}(t_0) s_{m,l}(t_0 + t)}{\sum_{\langle m,l \rangle} s_{m,l}(t_0)}, \quad (2)$$

where the set of values $\{s_{m,l}(t)\}$ form the connectivity matrix (defined elsewhere^{27,36}) at time *t*. If a

bond exists between molecules *m* and *l* at time *t*₀ and exists continuously until time *t* at which point it breaks, for all subsequent times *s*_{*m,l*}(*t*) is considered to be zero even though the bond may reform. This special case of *C*_{HB}(*t*) is called the continuous hydrogen bond autocorrelation function, *C*_{HB,c}(*t*). We calculated *C*_{HB,c}(*t*) for TJE and SPC water at various state points. These autocorrelation functions decay in an approximately exponential manner,

$$C_{\text{HB,c}}(t) = \exp(-t/\tau_{\text{HB}}). \quad (3)$$

The continuous hydrogen bond autocorrelation function decay constant, τ_{HB} , was calculated by a least squares fit of the corresponding *C*_{HB,c}(*t*) curve of each water model. These decay constants are plotted against density at 773 K in Figure 5. The estimated uncertainties in these decay constants are less than ±7% at a 95% confidence level. The decay times decrease with increasing density and do so more dramatically at low densities. At a

**FIGURE 4.** Hydrogen bonded cluster size distributions for TJE and SPC water models at 773 K.**FIGURE 5.** Variation of hydrogen bonding autocorrelation decay times with density at 773 K for TJE and SPC water models under supercritical conditions.

given temperature higher densities translate into more frequent collisions between a bonded pair and other molecules, resulting in an increase in the rate of bond breakage. The SPC model exhibits smaller decay times and hence more frequent rupture of hydrogen bonds than the TJE model for the same state point. This occurs because the flexible model allows distorted hydrogen bonding configurations, while even small perturbations of a hydrogen bonded rigid pair may result in pair geometries that have non-hydrogen-bonding pair energies. The slope of the data points for the SPC model is clearly larger than for the TJE model, indicating that the hydrogen bond decay times for the rigid model are more sensitive to density. The temperature dependence of τ_{HB} for both models was reported previously.²⁷ Both models exhibit similar monotonic declines in τ_{HB} with temperature, although again, the SPC model has shorter decay times.

STRUCTURAL PROPERTIES

Figures 6 and 7 depict the pair correlation functions obtained from molecular dynamics simulations of TJE and SPC water at a low density and a high density supercritical condition. Comparison of the plots reveals that at low densities the flexible water model produces much sharper features in the pair correlation functions. Contrarily, at high densities the models give indistinguishable pair correlation functions. At intermediate densities the differences between the structures produced by these two models are intermediate between these two cases.

Enhanced structure in pair correlation functions from rigid water models has been associated with the dipole moment of the model molecule. For example figures 2 and 4 of Chialvo and Cummings³⁸ show that enhanced structure accompanies higher dipole moments for SPC models with different atomic charges. Dipole moments alone, however, are not sufficient to explain the trends in the pair correlation functions we observed with the TJE and SPC models. For example, at high densities the average dipole moments differ the most, yet the pair correlation functions are indistinguishable. As the density is lowered and the dipole moments of the flexible and rigid models approach each other, however, the structural difference between them becomes more pronounced. Thus, rationalizations based only on dipole moments are inadequate when flexibility is involved.

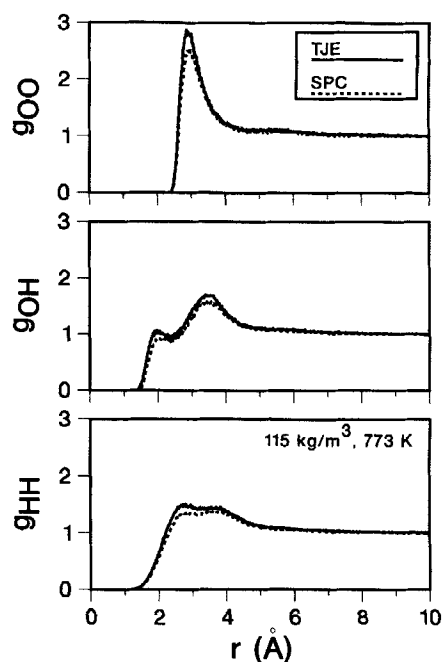


FIGURE 6. Pair correlation functions of supercritical water for TJE and SPC models at 773 K and 115 kg/m³.

At this point, we can only speculate as to the reason behind this difference in structure between the rigid and flexible models at low densities. We offer the following possible explanation without any direct proof. The peaks observed in Figures 6

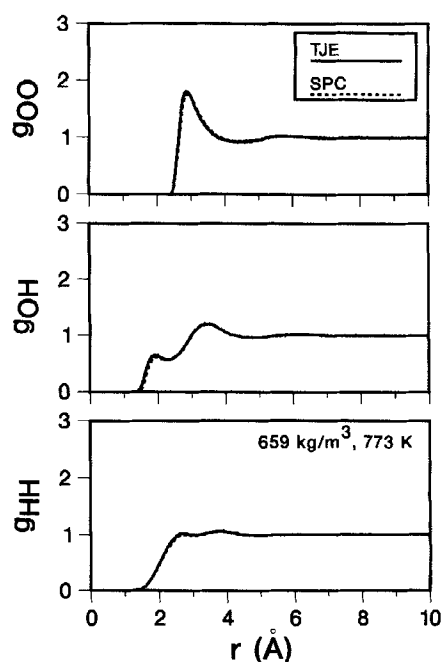


FIGURE 7. Pair correlation functions of supercritical water for TJE and SPC models at 773 K and 659 kg/m³.

and 7 correspond to molecules that are nearest neighbors of the reference molecule. The structure observed in the pair correlation functions is attributable primarily to molecules at small separations, such as molecules in clusters, rather than molecules that are far apart. At low densities, the clusters of water molecules that exist, are most likely dimers. Hence, we may envision pairs of molecules translating or rotating together. When any member of a pair of rigid molecules has a motion relative to the other member, this motion drives it out of the most probable configurations that contribute to the peaks in the structure. On the other hand, when a flexible molecule rotates or translates relative to its partner, it is plausible that it may contort in concert with its partner and thus keep the atoms at the most probable distances (possibly corresponding to energetically favorable hydrogen bonded geometries) for a greater length of time than would be possible for rigid molecules. At high densities where clusters would often have more than two members, such cooperative internal motion between any two nearest neighbor members would suffer interference from the presence of other molecules in the cluster. Thus, the possibility of nearest neighbor molecules bending or stretching in concert and producing the peak enhancement of the flexible model over the rigid model is diminished at higher densities.

There exist only very limited experimental results with which to compare the calculated pair correlation functions. A neutron diffraction with isotopic substitution (NDIS) study showed that the first peak of the g_{OH} pair correlation function is suppressed in SCW at 660 kg/m³ and 673 K.^{39,40} This result is not consistent with our simulations. Chialvo and Cummings³⁸ found that at supercritical conditions, the NDIS results for the g_{OH} pair correlation function were matched better by the SPCG⁴¹ water model than by the SPCE⁴² model, presumably because of the lower dipole moment of the SPCG model. The SPCG model is identical to the rigid SPC potential model, but with its point charges scaled to reproduce the gas-phase dipole moment of the water molecule, 1.85 D. The SPCE model is also identical to the SPC model except that the charges on the atoms are made slightly larger to account for self-energy attributable to polarization in the liquid state. The dipole moments of SPC and SPCE water are 2.27 and 2.35 D, respectively. These larger dipole moments allow the SPC and SPCE models to simulate liquid-phase

properties well, because it is at liquid densities that one might expect large polarization effects to result in effective dipole moments larger than the gas-phase value. Although it is plausible that at supercritical conditions polarization would play a smaller role than in liquid water, hence supporting the idea of water model with a gaslike dipole moment, there are sound reasons for favoring a model with a higher dipole moment. First, reducing the dipole moment results in an increase in the simulated pressure so that the thermodynamic properties of SCW are poorly represented. In fact, among the rigid SPC models, the SPCE model, which has the highest dipole moment, best reproduces the critical point of water.⁴³ Second, evidence suggesting that the dipole moment of dense SCW is higher than the gas-phase value comes from ab initio molecular dynamics simulations of SCW⁴⁴ which show the dipole moment to be 2.3 ± 0.2 D at 640 kg/m³ and 730 K. Thus, although the SPCG model gives better agreement with the NDIS results, it is not likely that simply scaling the charges on an SPC-like model will lead to a potential function that faithfully predicts other properties of SCW.

To summarize this section we note that the flexible model does no worse than the rigid model in comparison to the NDIS experiments at high densities. At low densities, where no experimental results are available, the flexible model produces a more enhanced structure. Any judgment on whether this behavior of the flexible model at low densities is better or worse than the rigid model will have to wait until experimental information at low densities becomes available.

DIELECTRIC PROPERTIES

The frequency-independent dielectric constant, ϵ_0 , may be calculated from simulations under reaction field conditions using the relation

$$\frac{(\epsilon_0 - 1)(2\epsilon_{RF} + 1)}{3(2\epsilon_{RF} + \epsilon_0)} = \frac{nG_k\langle\mu^2\rangle}{9k_B T\epsilon_0}, \quad (4)$$

where n is the number density, ϵ_0 is the permittivity of free space, and G_k , the finite system analog of the Kirkwood g factor, is given by

$$G_k = \frac{\langle M^2 \rangle}{N\langle\mu^2\rangle}, \quad (5)$$

with \mathbf{M} being the total dipole moment of a system of N molecules. We calculated the dielectric constants for the TJE and SPC models at 10 supercritical state points. The results are summarized in Figures 8 and 9.

Figure 8 shows the variation of the dielectric constant, ϵ_0 , with density at 773 K. It is evident that the SPC model underestimates ϵ_0 at high densities, while the TJE model reproduces the experimental trends reasonably well over the entire range of densities. The upper and lower panels of Figure 9 depict the temperature dependence of ϵ_0 at two densities (257 and 659 kg/m³, respectively). Again, the TJE model follows the experimental values fairly well over a wide range of temperature at both densities. The SPC model does very well at the low density, but underestimates the high density ϵ_0 curve over the entire range of temperatures. Moreover, the slope of the curve for the SPC model is smaller than the slope of the experimental curve at this high density. Clearly, the flexible potential model, because of its attendant ability to change its dipole moment with density, tracks the experimental values of the dielectric constant in a superior manner.

Tables IV and V list the ϵ_0 and G_k values at various state conditions. The uncertainties in the tables are the standard deviations. It is evident that even for the high temperature, low density condition of 1073 K and 257 kg/m³, the G_k value is 1.39 for both water models. For a fluid with a completely random orientation of molecules, G_k would be unity. Thus, even at this rarefied super-

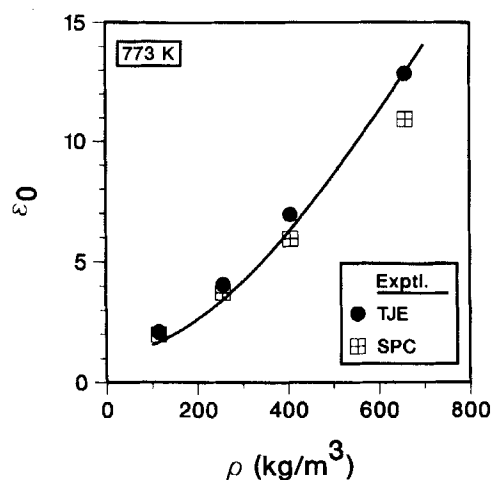


FIGURE 8. Dielectric constants of supercritical water for TJE and SPC models at 773 K. Experimental values.⁴⁵

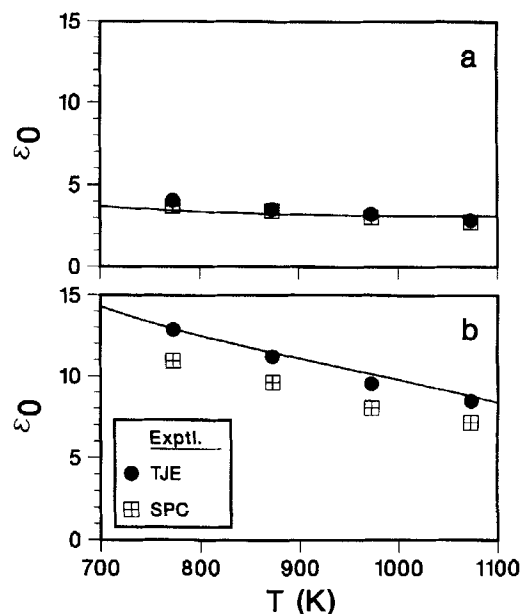


FIGURE 9. Dielectric constants of supercritical water for TJE and SPC models at (a) 257 kg/m³ and (b) 659 kg/m³. Experimental values.⁴⁵

critical condition with high kinetic energy there is a considerable amount of angular correlation.

SELF-DIFFUSIVITY

Figure 10 compares self-diffusivities, D , for the TJE and SPC water models at 773 K and various densities with the experimental data of Lamb et al.⁴⁶ The self-diffusivities were calculated from

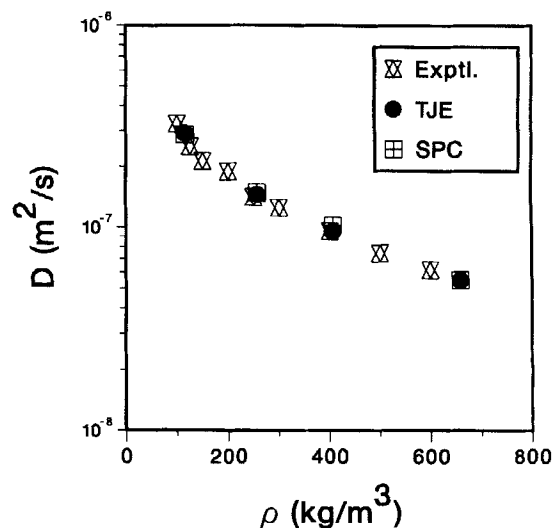


FIGURE 10. Comparison of self-diffusivities of SPC and TJE water at 773 K with experimental values.⁴⁶

TABLE IV.
Molecular and Collective Properties of Supercritical Water at 257 kg / m³.

Property	State 2a		State 2b		State 2c		State 2d	
	TJE	SPC	TJE	SPC	TJE	SPC	TJE	SPC
T (K)	773		873		973		1073	
$\langle r_{OH} \rangle$ (Å)	1.006 ± 0.002	1.0	1.006 ± 0.002	1.0	1.006 ± 0.002	1.0	1.006 ± 0.003	1.0
$\langle \theta_{HOH} \rangle$ (degree)	107.3 ± 0.4	109.5	107.4 ± 0.5	109.5	107.5 ± 0.5	109.5	107.6 ± 0.6	109.5
$\langle \mu \rangle$ (D)	2.35 ± 0.01	2.27	2.34 ± 0.01	2.27	2.34 ± 0.02	2.27	2.34 ± 0.02	2.27
G _k	1.61 ± 0.01	1.54 ± 0.01	1.51 ± 0.01	1.55 ± 0.01	1.50 ± 0.02	1.46 ± 0.01	1.39 ± 0.01	1.39 ± 0.01
ϵ_0	4.07 ± 1.02	3.73 ± 1.01	3.53 ± 1.01	3.43 ± 1.01	3.25 ± 1.02	3.04 ± 1.01	2.88 ± 1.02	2.76 ± 1.01
Exptl ⁴⁵ ϵ_0	3.45		3.24		3.15		3.13	

TABLE V.
Molecular and Collective Properties of Supercritical Water at 659 kg / m³.

Property	State 4a		State 4b		State 4c		State 4d	
	TJE	SPC	TJE	SPC	TJE	SPC	TJE	SPC
T (K)	773		873		973		1073	
$\langle r_{OH} \rangle$ (Å)	1.009 ± 0.002	1.0	1.009 ± 0.002	1.0	1.009 ± 0.002	1.0	1.009 ± 0.002	1.0
$\langle \theta_{HOH} \rangle$ (degree)	106.1 ± 0.5	109.5	106.3 ± 0.5	109.5	106.3 ± 0.5	109.5	106.4 ± 0.5	109.5
$\langle \mu \rangle$ (D)	2.39 ± 0.01	2.27	2.38 ± 0.01	2.27	2.38 ± 0.01	2.27	2.38 ± 0.02	2.27
G _k	2.23 ± 0.03	2.09 ± 0.04	2.19 ± 0.01	2.06 ± 0.03	2.06 ± 0.01	1.90 ± 0.01	2.00 ± 0.02	1.84 ± 0.01
ϵ_0	12.87 ± 1.14	10.94 ± 1.18	11.20 ± 1.04	9.61 ± 1.11	9.55 ± 1.05	8.03 ± 1.03	8.46 ± 1.07	7.15 ± 1.04
Exptl ⁴⁵ ϵ_0	12.92		11.45		10.14		8.78	

the mean-square displacement of the center of mass of the molecule as

$$D = \frac{1}{6N} \lim_{t \rightarrow \infty} \frac{d}{dt} \left\langle \sum_{m=1}^N [\mathbf{r}_i(t) - \mathbf{r}_i(0)]^2 \right\rangle. \quad (6)$$

The mean-square displacements were averaged over time origins 500 fs apart with a maximum delay time of 10 ps. The self-diffusivities were then obtained from the long time slopes of the mean-square displacements. The estimated uncertainties in these self-diffusivities are less than $\pm 10\%$ for the flexible model and less than $\pm 1\%$ for the rigid model at a 95% confidence level. It is evident that the potential model used, whether TJE or SPC, does not influence the simulation results, which are in excellent agreement with the experiment. A similar observation was made by Kalinichev²⁶ who also calculated self-diffusivity of SCW using a completely different potential model.

POWER SPECTRA

We calculated the velocity autocorrelation functions for the hydrogen atoms of the TJE and SPC water models from velocity data collected from simulations conducted in the microcanonical ensemble at 257 kg/m³ and 773 K. The average temperatures for the flexible and rigid simulations were 768 and 770 K, respectively. The normalized velocity autocorrelation function is defined as⁴⁷

$$C_v(t) = \frac{\langle v(0) \cdot v(t) \rangle}{\langle v(0) \cdot v(0) \rangle}. \quad (7)$$

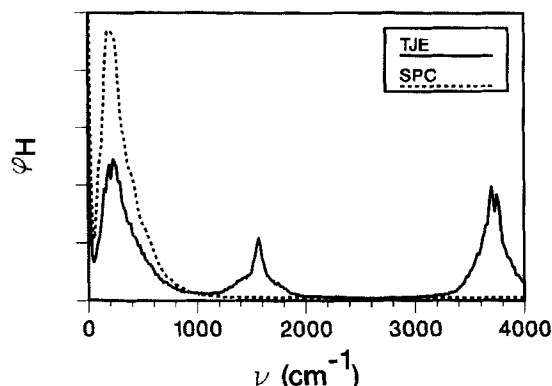


FIGURE 11. Comparison of the power spectra of SPC and TJE water at 257 kg/m³ and 773 K (units of ϕ_H are arbitrary).

The Fourier transform of the velocity autocorrelation function yields the power spectrum as

$$\varphi(\nu) = 2\pi c \int_0^\infty C_v \cos(2\pi c \nu t) dt, \quad (8)$$

where ν is the wavenumber and c is the velocity of light. In our calculations the fast Fourier transform method⁴⁸ was used for this purpose. The power spectra for the two water models are shown in Figure 11. The TJE model exhibits peaks for the bending and stretching motions of the water molecule at around 1600 and 3700 cm⁻¹, respectively, which the rigid model is incapable of producing. The rotational or perhaps librational structure centered at around 200 cm⁻¹ is common to both water models.

Conclusions

CW was simulated at 10 state points using both rigid and flexible water potentials. The flexible TJE model exhibited superior characteristics for a number of properties, including the simulated pressure and the dielectric constant. The pair correlation functions of the flexible model were slightly enhanced at low densities in comparison to the rigid SPC model. With regard to the PVT trends, the agreement of our simulated state points with the experimental isotherm is excellent for both models at low densities but deteriorates at high densities. This deterioration in agreement with the experiment is greater for the rigid SPC model. The TJE model shows greater fidelity than the SPC model to the trends and values of the experimental dielectric constants of SCW over a wide range of temperatures and densities. Both models do equally well in reproducing the self-diffusivity of SCW. No significant difference was found in the positions of the libration/rotation peak of the power spectra of the two water models. The TJE model shows more hydrogen bonding than the SPC model, although the cluster size distributions are very similar. Hydrogen bonds break more readily for the rigid model. Computationally, the TJE model is no more demanding than the rigid SPC model, if the r-RESPA method is utilized.

The favorable features of the TJE model may be attributed to its ability to respond to its environment by a change in geometry and hence dipole moment. While flexibility is clearly desirable, the TJE model has, on average, too high a dipole moment to reproduce the first peak of the g_{OH} of SCW accurately. Even the rigid SPC model, with a

slightly smaller dipole moment, fails in this regard. At the same time, the SPCE water model,⁴² which has a higher dipole moment than the plain SPC model, reproduces the critical point of real water more accurately than the latter model.⁴³ Thus, there is a dichotomy between the desirable effect of a large dipole moment in reproducing the PVT behavior of real SCW and the unwanted enhancing effect that a large dipole moment has on the structure of SCW. It is not clear that simple potential models such as the SPC, the SPCE, or the TJE models can satisfactorily address both these issues simultaneously. Whether these issues will be resolved by some combination of intermolecular interaction parameters, flexibility, and polarizability on an SPC type model or whether a higher level of theory such as the Car-Parrinello approach⁴⁹ will need to be invoked is not yet clear. The former approach is more desirable because it is computationally less demanding. The latter method, it is claimed, is more successful insofar as it addresses the structural issue,⁴⁴ although its large computational overhead means that it can only be applied to small systems (32 water molecules). In any event, these issues will continue to be the subjects of active research in the near future.

Nomenclature

C_v	velocity autocorrelation function
D	diffusivity, m^2/s
G_k	finite system analog of g factor
\mathbf{M}	collective dipole moment, D
N	number of molecules
N_m	number of molecules
N_a	number of atoms
P	pressure, bar
T	temperature, K
S_N	cumulative number fraction of clusters of size N
U	energy, kJ/mol
V	system volume, m^3
c	velocity of light, m/s
g	atom-atom pair correlation function
\mathbf{k}	reciprocal lattice vector, m^{-1}
k_B	Boltzmann constant, J/K
n	number density, m^{-3}
n_{HB}	hydrogen bonds per water molecule
\mathbf{n}	lattice vector, m
q	charge, e
r	distance, Å

t	time, s
v	velocity, m/s

GREEKS

α	Ewald separation parameter, m^{-1}
ϵ_0	dielectric constant
κ	intramolecular atomic index
λ	intramolecular atomic index
ϵ_0	permittivity of free space
μ	dipole moment, D
ν	wavenumber, cm^{-1}
φ	power spectrum
ρ	density, kg/m^3
τ	decay constant, ps
θ	bond angle, degrees

SUBSCRIPTS

H	hydrogen
O	oxygen
RF	reaction field
inter	intermolecular
intra	intramolecular
i	atomic index
j	atomic index
l	molecular index
m	molecular index

References

1. A. Rahman and F. Stillinger, *J. Chem. Phys.*, **55**, 3336 (1971).
2. A. Kalinichev, *Int. J. Thermophys.*, **7**, 887 (1986).
3. A. Kalinichev, *Z. Naturforsch.*, **46a**, 433 (1991).
4. P. Cummings, H. Cochran, J. Simonson, R. Mesmer, and S. Karaborni, *J. Chem. Phys.*, **94**, 5606 (1991).
5. T. Mizan, P. Savage, and R. Ziff, *J. Phys. Chem.*, **98**, 13067 (1994).
6. P. Savage, S. Gopalan, T. Mizan, C. Martino, and E. Brock, *AIChE J.*, **41**, 1723 (1995).
7. R. Mountain, *J. Chem. Phys.*, **90**, 1866 (1989).
8. H. Cochran, P. Cummings, and S. Karaborni, *Fluid Phase Equilib.*, **71**, 1 (1992).
9. J. Gao, *J. Am. Chem. Soc.*, **115**, 6893 (1993).
10. P. Balbuena, K. Johnston, and P. Rossky, *J. Am. Chem. Soc.*, **116**, 2689 (1994).
11. P. Cummings, A. Chialvo, and H. Cochran, *Chem. Eng. Sci.*, **49**, 2735 (1994).
12. S. Cui and J. Harris, *Chem. Eng. Sci.*, **49**, 2749 (1994).
13. J. Seminario, M. Concha, J. Murray, and P. Politzer, *Chem. Phys. Lett.*, **222**, 25 (1994).
14. P. Balbuena, K. Johnston, and P. Rossky, *J. Phys. Chem.*, **99**, 1554 (1995).

15. L. Flanagan, P. Balbuena, K. Johnston, and P. Rossky, *J. Phys. Chem.*, **99**, 5196 (1995).
16. H. Berendsen, J. Potsma, W. van Gunsteren, and J. Hermans, *Intermolecular Forces*, D. Reidel Publishing Co., Dordrecht, Netherlands, 1981, p. 331.
17. W. Jorgensen, J. Chandrasekhar, J. Madura, R. Impey, and M. Klein, *J. Chem. Phys.*, **79**, 926 (1983).
18. A. Wallqvist and O. Teleman, *Mol. Phys.*, **74**, 515 (1991).
19. A. Rahman, H. Lemberg, and F. Stillinger, *J. Chem. Phys.*, **63**, 5223 (1975).
20. F. Stillinger and A. Rahman, *J. Chem. Phys.*, **68**, 666 (1978).
21. G. Jancso, P. Bopp, and K. Keinzinger, *Chem. Phys.*, **85**, 377 (1984).
22. K. Toukan and A. Rahman, *Phys. Rev. B*, **31**, 2643 (1985).
23. G. Lie and E. Clementi, *Phys. Rev. A*, **33**, 2679 (1986).
24. L. Dang and B. Pettitt, *J. Phys. Chem.*, **91**, 3349 (1987).
25. O. Teleman, B. Jönsson, and S. Engström, *Mol. Phys.*, **60**, 193 (1987).
26. A. Kalinichev, *Ber. Bunsenges. Phys. Chem.*, **97**, 872 (1993).
27. T. Mizan, P. Savage, and R. Ziff, *J. Phys. Chem.*, **100**, 403 (1996).
28. M. Tuckerman, B. Berne, and G. Martyna, *J. Chem. Phys.*, **97**, 1990 (1992).
29. D. Eisenberg and W. Kauzmann, *The Structure and Properties of Water*, Oxford University Press, Oxford, U.K., 1969.
30. M. Allen and D. Tildesley, *Computer Simulation of Liquids*, Oxford University Press, Oxford, U.K., 1987.
31. H. Berendsen, J. Potsma, W. van Gunsteren, A. DiNola, and J. Haak, *J. Chem. Phys.*, **81**, 3684 (1984).
32. H. Andersen, *J. Comp. Phys.*, **52**, 24 (1983).
33. S. Nosé and M. Klein, *Mol. Phys.*, **50**, 1055 (1983).
34. K. Refson, *Moldy User's Manual, Revision: 2.6*, Oxford University, Oxford, 1994.
35. L. Haar, J. Gallagher, and G. Kell, *NBS / NRC Steam Tables*, Hemisphere Publishing Corp., Washington, D.C., 1984.
36. T. Mizan, P. Savage, and R. Ziff, *ACS Symp. Ser.*, **608**, 47 (1995).
37. D. Rapaport, *Mol. Phys.*, **50**, 1151 (1983).
38. A. Chialvo and P. Cummings, *J. Chem. Phys.*, **101**, 4466 (1994).
39. P. Postorino, R. Tromp, M.-A. Ricci, A. Soper, and G. Neilson, *Nature*, **366**, 668 (1993).
40. R. Tromp, P. Postorino, G. Neilson, M. Ricci, and A. Soper, *J. Chem. Phys.*, **101**, 6210 (1994).
41. H. Strauch and P. Cummings, *J. Chem. Phys.*, **96**, 864 (1992).
42. H. Berendsen, J. Grigera, and T. Straatsma, *J. Phys. Chem.*, **91**, 6269 (1987).
43. Y. Guissani and B. Guillot, *J. Chem. Phys.*, **98**, 8221 (1993).
44. E. Fois, M. Sprik, and M. Parrinello, *Chem. Phys. Lett.*, **223**, 411 (1994).
45. M. Uematsu and E. Franck, *J. Phys. Chem. Ref. Data*, **9**, 1291 (1980).
46. W. Lamb, G. Hoffman, and J. Jonas, *J. Chem. Phys.*, **74**, 6875 (1981).
47. J. Haile, *Molecular Dynamics Simulation: Elementary Methods*, Wiley, New York, 1992.
48. W. Press, B. Flannery, S. Teukolsky, and W. Vetterling, *Numerical Recipes*, Cambridge University Press, London, U.K., 1986.
49. R. Car and M. Parrinello, *Phys. Rev. Lett.*, **55**, 2471 (1985).